Structure of Rabbit Muscle Pyruvate Kinase Complexed with Mn^{2+}, K^+, and Pyruvate[†,‡]

Todd M. Larsen, L. Timothy Laughlin, Hazel M. Holden, Ivan Rayment, and George H. Reed*

Institute for Enzyme Research, Graduate School, and Department of Biochemistry, College of Agricultural and Life Sciences, University of Wisconsin—Madison, Madison, Wisconsin 53705

Received January 5, 1994; Revised Manuscript Received March 25, 1994[⊗]

ABSTRACT: The molecular structure of rabbit muscle pyruvate kinase, crystallized as a complex with Mn^{2+}, K^+, and pyruvate, has been solved to 2.9-Å resolution. Crystals employed in the investigation belonged to the space group *P*1 and had unit cell dimensions a = 83.6 Å, b = 109.9 Å, c = 146.8 Å, α = 94.9°, β = 93.6°, and γ = 112.3°. There were two tetramers in the asymmetric unit. The structure was solved by molecular replacement, using as the search model the coordinates of the tetramer of pyruvate kinase from cat muscle [Muirhead, H., Claydon, D. A., Barford, D., Lorimer, C. G., Fothergill-Gilmore, L. A., Schiltz, E., & Schmitt, W. (1986) *EMBO J. 5,* 475–481]. The amino acid sequence derived from the cDNA coding for the enzyme from rabbit muscle was fit to the electron density. The rabbit and cat muscle enzymes have ~94% sequence identity, and the folding patterns are expected to be nearly identical. There are, however, three regions where the topological models of the cat and rabbit pyruvate kinases differ. Mn^{2+} coordinates to the protein through the carboxylate side chains of Glu 271 and Asp 295. These two residues are strictly conserved in all known pyruvate kinases. In addition, the density for Mn^{2+} is connected to that of pyruvate, consistent with chelation through a carboxylate oxygen and the carbonyl oxygen of the substrate. The ϵ-NH_2 of Lys 269 and the OH of Thr 327 lie on either side of the methyl group of bound pyruvate. Spherical electron density, assigned to K^+, is located within a well-defined pocket of four oxygen ligands contributed by the carbonyl oxygen of Thr 113, O^{γ} of Ser 76, $O^{\delta 1}$ of Asn 74, and $O^{\delta 2}$ of Asp 112. The interaction of Asp 112 with the side chains of Lys 269 and Arg 72 may mediate, indirectly, monovalent cation effects on activity.

Pyruvate kinase (EC 2.7.1.40) catalyzes the reaction of ADP, P-enolpyruvate,[1] and a proton to give ATP and pyruvate. This enzyme has been the subject of enzymological and biophysical investigations for over 50 years (Boyer, 1962; Kayne, 1973; Nowak & Suelter, 1981). Pyruvate kinase was the first enzyme for which a dependence of the activity on monovalent cations was documented (Boyer et al., 1942). An intriguing requirement for activation of the enzyme by 2 equiv of divalent cation was documented much later (Gupta et al., 1976; Gupta & Mildvan, 1977; Baek & Nowak, 1982).

By now, there is much evidence to suggest that the physiological reaction of pyruvate kinase takes place in two steps. The first step is phosphoryl transfer from P-enolpyruvate to ADP to give the bound enolate of pyruvate and ATP (Seeholzer et al., 1991). In the second step, a proton is added to the 2 *si* face of the enolate to produce the keto form of pyruvate (Rose, 1970; Kuo & Rose, 1978; Kuo et al., 1979). The highly favorable ketonization renders the overall reaction exergonic, to the extent that the reaction is metabolically irreversible. The enzyme has a number of interesting side activities, including ATP- and bicarbonate-dependent ATPase, phosphorylation of fluoride (Tietz & Ochoa, 1958) and hydroxylamine (Kupiecki & Coon, 1960; Weiss et al., 1984), ATP-dependent phosphorylation of glycolate (Kayne, 1974) and other α-hydroxy or α-thiol carboxylates (Ash et al., 1984), and decarboxylation of oxaloacetate (Creighton & Rose, 1976).

All known pyruvate kinases are tetrameric proteins of MW ~237 000. In cells or tissues, where P-enolpyruvate is required for other functions or for gluconeogenesis, the enzyme is typically regulated by metabolites that serve as allosteric effectors (Hall & Cottam, 1978). In addition, the L isozyme from liver is regulated by the phosphorylation of a specific serine residue located on an extended N-terminus (Ljungstrom et al., 1976). The muscle isozyme (M_1) is a homotetramer that lacks the phosphorylation site. Under normal assay conditions, the subunits of the muscle isozyme function independently, and the activity is not markedly affected by other glycolytic intermediates (Kayne, 1973). The enzyme does, however, exhibit cooperative behavior in the presence of phenylalanine, although the physiological significance of this phenomenon is not yet clear (Carminatti et al., 1971).

The three-dimensional structure of the apoenzyme from cat skeletal muscle was solved to high resolution by Muirhead and co-workers several years ago (Stammers et al., 1975; Stuart et al., 1979; Muirhead et al., 1987). Each subunit was shown to consist of an intricate four-domain motif, wherein the active site was located in a cleft between the two largest domains, the eight-stranded β-barrel of domain A and domain B. Gd^{3+}, one of the heavy-atom derivatives employed for the structural investigation, bound at a position believed to be a binding site for one of the essential divalent cations. Other regions that were suggested as potential sites of interaction between the protein and substrates or cofactors were surmised on the basis

[†] This research was supported in part by NIH Grants GM35752 (G.H.R.), GM39082 and HL42322 (H.M.H.), and AR35186 (I.R.).

[‡] X-ray coordinates for the rabbit muscle protein have been deposited in the Brookhaven Protein Data Bank under file name 1PKN.

* Address correspondence to this author at the Institute for Enzyme Research, University of Wisconsin, 1710 University Ave., Madison, WI 53705. Telephone: 608-262-0509. FAX: 608-265-2904.

[⊗] Abstract published in *Advance ACS Abstracts,* May 1, 1994.

[1] Abbreviations: P-enolpyruvate, phosphoenolpyruvate; PCR, polymerase chain reaction; PEG, poly(ethylene glycol); Hepes, 4-(2-hydroxyethyl)-1-piperazineethanesulfonic acid; EPR, electron paramagnetic resonance; NMR, nuclear magnetic resonance.

0006-2960/94/0433-6301$04.50/0 © 1994 American Chemical Society

of X-ray data obtained from crystals soaked in the respective ligand solutions (Muirhead et al., 1986). The resolution of ~6 Å for these X-ray data sets, however, limited the structural details obtained from such soaking experiments (Stammers et al., 1975). In addition, high concentrations of ammonium sulfate in the mother liquor apparently interfered with the binding of the ionic substrates and activators, such that the occupancies of the respective sites were low. Consequently, the assignment of roles for specific amino acid side chains in substrate binding and catalysis remains tentative, and structural details that might aid in the interpretation of more recent functional measurements, such as the ^3H trapping experiments (Rose & Kuo, 1989; Rose et al., 1991), are presently lacking. In addition, the earlier studies on cat muscle pyruvate kinase were performed at a time when least-squares refinement of protein structures was not routine for a molecule of this size. Since that time, improvements in the speed and capacity of computers and molecular graphics allow these models to be refined and justify a reexamination of the structure.

Recently, crystallization and preliminary X-ray characterization of the Mn^{2+}–pyruvate and Mn^{2+}–oxalate complexes of rabbit muscle pyruvate kinase were reported (Schmidt-Bäse et al., 1991). These crystals diffract to high resolution, and the nonionic precipitant, PEG 8000, does not interfere with ligand and cofactor binding. The present article reports the three-dimensional structure of the liganded subunit of pyruvate kinase from rabbit muscle. The amino acid sequence for this enzyme, inferred from the sequence of the respective cDNA, is also reported. X-ray coordinates for the rabbit muscle protein have been deposited in the Brookhaven Protein Data Bank (Bernstein et al., 1977).

EXPERIMENTAL PROCEDURES

Materials for DNA Manipulation. Restriction endonucleases and DNA polymerase 1 were purchased from New England Biolabs. *Taq* polymerase and DNAse 1 were purchased from Boehringer Mannheim. Helper phage R408 was obtained from Promega. Tryptone and yeast extract were obtained from Difco. Oligonucleotides were synthesized at local facilities.

^{32}P Labeling of the Rat Pyruvate Kinase M1 Gene. The rat muscle pyruvate kinase gene was excised from the plasmid pCJ22 (Parkison et al., 1991) with the restriction endonucleases, *Nde*I and *Eco*RI. This plasmid was a generous gift from Dr. C. Parkison (LMB, NCI, NIH, Bethesda, MD). The gene for rat pyruvate kinase was purified on an agarose gel and labeled with ^{32}P by DNA polymerase 1 using a nick translation protocol (Sambrook et al., 1989). [^{32}P]dCTP (250 μCi, >3 × 10^3 Ci/mmol, DuPont-NEN, Boston, MA) was used to label 100 ng of the rat pyruvate kinase gene to a specific activity of 1.4 × 10^9 cpm/μg.

Screening of the cDNA Library from Rabbit Muscle. A cDNA library prepared from rabbit skeletal muscle mRNA was generously provided by the laboratory of Dr. Neil Madsen (University of Alberta, Edmonton, AB, Canada). The library was packaged into the LamdaZap II vector (Stratagene, La Jolla, CA) and subsequently plated out at high plaque density, ~2 × 10^4/plate, on five plates with *Escherichia coli* XL1-Blue (Stratagene) as the host strain. Duplicate phage plaques were transferred to Hybond-N nylon filters (Amersham), denatured, neutralized, rinsed, and fixed according to the manufacturer's protocol. The filters were placed in a prehybridization solution of 50% formamide, 0.9 M NaCl, 60 mM NaH_2PO_4, 6 mM EDTA, and 0.05% Blotto for 3.5 h at 42 °C. A solution containing the ^{32}P-labeled gene of rat pyruvate kinase was boiled for 10 min and then added directly to the prehybridization solution. Hybridization was carried out at 42 °C for 16 h with shaking. The filters were subsequently washed four times in a solution of 0.3 M NaCl, 20 mM NaH_2PO_4, 2 mM EDTA, and 0.1% SDS for 5 min per wash at room temperature. The filters were then washed for 2.5 h in 0.15 M NaCl, 10 mM NaH_2PO_4, 2 mM EDTA, and 0.1% SDS, followed by a 2.5-h soak in 15 mM NaCl, 1 mM NaH_2PO_4, 0.1 mM EDTA, and 0.1% SDS. The filters were placed on film with intensifying screens at −70 °C for 12 h prior to development. Positive plaques were selected and repeatedly replated at lower plaque densities until individual, pure positive plaques were obtained.

Identification of the Rabbit Muscle Pyruvate Kinase Gene. The pBluescript phagemids containing the library inserts were excised from the LambdaZap II phage by coinfecting XL1-Blue cells with positive phage stocks and R408 helper phage. The pBluescript phagemid particles were produced and used to infect XL1-Blue cells, which were then plated out on LB–ampicillin plates and grown overnight (Short et al., 1988). Colonies were picked and cultured in LB–ampicillin liquid medium. The pBluescript plasmid was purified using the Magic Miniprep system (Promega). Identification of the positive inserts was accomplished by PCR. The following primers were synthesized:

1 5′-TAY ATG GAR AAR TGY GA-3′

2 5′-CCD ATC ATC ATY TTY TG-3′

3 5′-CAR AAR ATG ATG ATH GG-3′

4 5′-TCR CAY TTY TCC ATR TA-3′

T3 5′-ATT AAC CCT CAC TAA AG-3′

T7 5′-AAT ACG ACT CAC TAT AG-3′

where Y is C or T, R is A or G, D is A, G, or T, and H is A, C, or T. Primers 1 and 4 are complementary to each other and were derived from the highly conserved amino acid sequence ^{147}YMEKCD from the rat pyruvate kinase gene. Likewise, primers 2 and 3 were derived from the highly conserved amino acid sequence ^{309}QKMMIG.

The PCR technique was used to determine the orientation and length of the positive inserts. A Perkin-Elmer thermocycler completed 40 cycles as follows: a melting temperature of 95 °C for 1 min; an annealing temperature of 42 °C for 45 s; and an extension temperature of 72 °C for 2 min. PCR conducted with primers 1 and 2 verified the identity of the pyruvate kinase gene. Primers 3 and 4, in conjunction with primers T3 and T7, were employed to determine the orientation and size of the gene in the phagemid.

A full-length positive clone was sequenced with the Sequenase v.2 Kit (U.S. Biochemical). A double-stranded phagemid served as the template, and the above primers were employed to sequence the pyruvate kinase clone. Additional primers were synthesized and used as needed to complete the sequencing.

Screening Results. The initial screen of the library yielded 32 positive plaques out of ~10^5. Eight of the 32 original positives were rescreened and plaque-purified. Gel analysis of the PCR products showed that one of the positive phagemid inserts was large enough to contain the entire coding region of the pyruvate kinase gene. The amino acid sequence of this clone was compared to the sequences of other pyruvate kinases by the Bestfit and Pileup programs of the GCG package (Devereux et al., 1984).

Table 1: Intensity Statistics for the Native X-ray Data Set

	overall	resolution range (Å)							
		100–7.62	–5.39	–4.41	–3.82	–3.41	–3.12	–2.89	–2.70
no. of measurements	168794	11173	22363	26301	27454	27716	26471	17874	9442
no. of independent reflections[a]	104618	5518 (3523)	10587 (7197)	13554 (8105)	15768 (7966)	17204 (7731)	18014 (6830)	13991 (3453)	9982 (180)
% of the theoretical no. of reflections	80	95	99	100	97	91	90	64	41
av intensity		1271	504	785	657	439	265	179	124
σ		112	67	92	88	77	67	64	50
R factor[b] (%)	10.8	5.6	9.2	8.2	9.7	12.9	19.1	26.6	28.7

[a] This is the number of reduced observations. Shown in parentheses is the number of independent measurements for which there were duplicate or symmetry-related observations. [b] R factor = $(\Sigma|I - \bar{I}|/\Sigma I) \times 100$.

Biochemical Methods. Pyruvate kinase was isolated from rabbit skeletal muscle according to the protocol of Tietz and Ochoa (1958). Gel filtration chromatography over Sephacryl S-300 was added as a final purification step (Ash et al., 1984). Single crystals ~0.8 × 0.5 × 0.1 mm were grown at room temperature, as described previously (Schmidt-Bäse et al., 1991), by the batch method. The crystallization solutions had the following composition, adjusted to pH 6.0: 2.9 mM pyruvate, 1.2 mM $MnCl_2$, 0.45 M KCl, 7.9–8.4% PEG 8000, 30 mM succinate, 6.4–7.0 mg mL^{-1} pyruvate kinase, and 4.3 mM Hepes. The crystals belong to the space group $P1$. The unit cell dimensions are a = 83.6 Å, b = 109.9 Å, c = 146.8 Å, α = 94.9°, β = 93.6°, and γ = 112.3°, and two tetramers make up the asymmetric unit. The presence of two tetramers in the crystallographic asymmetric unit raises the question of whether or not the space group might be $C2$ rather than $P1$. Examination of the orientation of the two independent molecules in the unit cell reveals that they are related to each other by a local 2-fold screw axis that lies parallel to the crystallographic a axis. This packing represents local symmetry since there is no crystallographic 2-fold axis observed along a, as evidenced by the appearance in the *hko* precession photograph (Schmidt-Bäse et al., 1991). Furthermore, attempts to index the data on a lattice with any higher symmetry were unsuccessful.

X-ray Data Collection and Processing. X-ray data were collected at 4 °C with a Siemens X1000D area detector system. The X-ray source was nickel-filtered copper Kα radiation from a Rigaku RU200 X-ray generator operated at 50 kV and 50 mA. These data were processed with the XDS data reduction software package (Kabsch, 1988a,b) and internally scaled according to the algorithm of Fox and Holmes (1966), as implemented by Dr. Phil Evans. The overall R factor, based on intensity, for the X-ray data set was 10.8%. Relevant X-ray data collection statistics may be found in Table 1. The X-ray data set was 80% complete to 2.7 Å.

Molecular Replacement. The three-dimensional structure of rabbit muscle pyruvate kinase was solved by molecular replacement using the software package, MERLOT (Fitzgerald, 1988). X-ray coordinates of the cat pyruvate kinase tetramer, kindly provided by Dr. Hilary Muirhead (University of Bristol, Bristol, UK), served as the search model. A cross-rotation function, calculated with X-ray data from 10 to 5.5 Å, revealed eight significant peaks, which could be further subdivided into two sets of four peaks. The peaks within each set were related to one another by rotations of 180°. Each set corresponded to a solution for one of the tetramers in the asymmetric unit. The Eulerian angles associated with these cross-rotation peaks were subsequently refined. One set of angles from each group was chosen for further calculations: α = 256.53°, β = 120.73°, γ = 303.96° (solution I); α = 54.25°, β = 60.94°, γ = 131.16° (solution II). The search model was rotated according to the Eulerian angles of solution I and translated by a = 0.00, b = 0.00, and c = 0.00, and the relationship between the two tetramers in the asymmetric unit was then established by holding the position of the first tetramer fixed, rotating the search model according to the Eulerian angles of solution II, and performing a translation function. A solution to the translation function was found at a = 0.67, b = 0.24, and c = 0.46, where the overall R factor dropped to 50.8%.

Electron Density Modification. Because there were two tetramers in the asymmetric unit, it was possible to improve the quality of the protein phases by the techniques of molecular averaging and solvent flattening (Bricogne, 1976). The eight rotational matrices relating the individual subunits in the asymmetric unit were determined from the positions of the cat pyruvate kinase coordinates, as obtained from the molecular replacement results. A molecular envelope was also generated from the X-ray coordinates of cat pyruvate kinase.

The initial electron density map employed in the averaging process was calculated to 4.5-Å resolution from reduced-bias coefficients of the form $(2m|F_o| - D|F_c|)$, where F_c refers to the calculated structure factor amplitudes based on the cat protein, and F_o refers to the observed structure factor amplitudes collected from the rabbit pyruvate kinase crystals. These coefficients were weighted (m and D) according to the SIGMA A algorithm of Read (1986). The averaging process was carried out for 15 cycles at 4.5-Å resolution, after which phase extension was performed from 4.5- to 2.9-Å resolution in steps of 0.006 $Å^{-1}$ reciprocal lattice units and a refinement of four cycles per step. Eighty-two refinement cycles were performed.

A model of the rabbit pyruvate kinase was built into this averaged electron density map using an Evans and Sutherland computer graphics system and the molecular modeling program, FRODO (Jones, 1985). Portions of the electron density associated with domain B were not well-defined in these initial maps. Upon completion of the chain tracing, the molecular model of the "averaged" subunit was placed back into the unit cell and subjected to four rounds of least-squares refinement using the computer package TNT (Tronrud et al., 1987). After each round of least-squares refinement, the phases were refined by cyclical molecular averaging for all of the measured data to 2.9-Å resolution. The global model for one subunit was then adjusted manually to fit the averaged electron density. The initial R factor was 39.3% for all measured X-ray data from 30 to 2.9 Å. Pyruvate, Mn^{2+}, and K^+ were not included in the refinement until completion of the fourth round.

Even though the electron density of domain B continued to improve with each round of refinement and model building, there were still several regions that remained ill-defined. Since we assumed that the B domains might adopt slightly different orientations according to their positions in the unit cell, the

Chart 1

```
1    SKSHSEAGSA FIQTQQLHAA MADTFLEHMC RLDIDSAPIT ARNTGIICTI
51   GPASRSVETL KEMIKSGMNV ARMNFSHGTH EYHAETIKNV RTATESFASD
101  PILYRPVAVA LDTKGPEIRT GLIKGSGTAE VELKKGATLK ITLDNAYMEK
151  CDENILWLDY KNICKVVDVG SKVYVDDGLI SLQVKQKGPD FLVTEVENGG
201  FLGSKKGVNL PGAAVDLPAV SEKDIQDLKF GVDEDVDMVF ASFIRKAADV
251  HEVRKILGEK GKNIKIISKI ENHEGVRRFD EILEASDGIM VARGDLGIEI
301  PAEKVFLAQK MIIGRCNRAG KPVICATQML ESMIKKPRPT RAEGSDVANA
351  VLDGADCIML SGETAKGDYP LEAVRMQHLI AREAEAAMFH RKLFEELARS
401  SSHSTDLMEA MAMGSVEASY KCLAAALIVL TESGRSAHQV ARYRPRAPII
451  AVTRNHQTAR QAHLYRGIFP VVCKDPVQEA WAEDVDLRVN LAMNVGKARG
501  FFKKGDVVIV LTGWRPGSGF TNTMRVVPVP *
```

next step was to examine visually all eight B domains as they appeared in the lattice. Electron density corresponding to the B domain was more ordered in subunits 2, 3, 6, and 7. Consequently, a cycle of density modification was conducted by averaging only these subunits. On the basis of this averaged electron density map, manual adjustments were made in the B domain to obtain the model described in this article. Thereafter, the B domain was returned to the cell and refined without any manual adjustments of the individual subunits in the crystallographic lattice. Apart from Mn^{2+}, K^+, and pyruvate, no other ions or solvent molecules were included in the refinement. An examination of the effects of crystal packing on the order of the individual subunits will be carried out once higher resolution data have been recorded. The current R factor is 19.1% for all measured X-ray data from 30 to 2.9 Å and root-mean-square deviations from "ideal" geometry of 0.011 Å for bond lengths, 2.8° for bond angles, and 0.006 Å for groups of atoms expected to be coplanar. A Ramachandran plot of main-chain dihedral angles is shown in Figure 1.

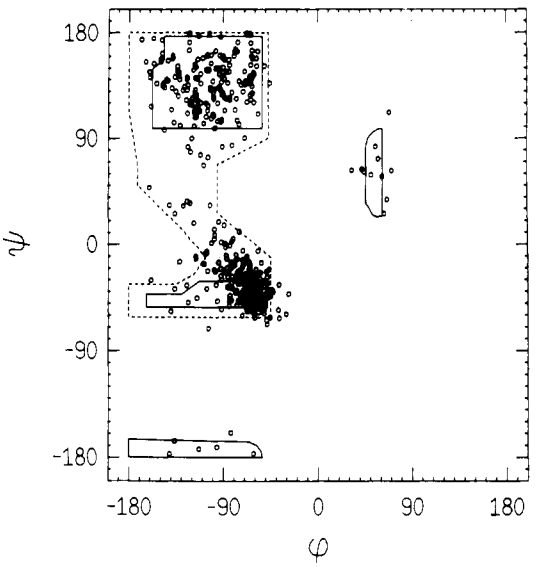

FIGURE 1: Ramachandran plot of main-chain dihedral angles. All non-glycinyl dihedral angles for the rabbit pyruvate kinase model are shown. Fully allowed ϕ,ψ values are enclosed by continuous lines; those only partially allowed are enclosed by broken lines.

RESULTS AND DISCUSSION

Amino Acid Sequence. The isolated clone coded for a protein sequence (530 amino acids) that was ~94% homologous to the M1 pyruvate kinases from cat and rat. The amino acid sequence inferred from the cloned gene is shown in Chart 1. Comparisons among the 20 known sequences for pyruvate kinases from a wide variety of organisms indicate that there is >39% identity and >54% similarity.

Electron Density Map. Representative portions of the averaged electron density map calculated to 2.9 Å are shown in Figure 2. For the most part, the electron density corresponding to backbone atoms was well-ordered, except for the 11 residues at the N-terminus and the region delineated by Ser 126 and Glu 132. These amino acid residues are not included in the present X-ray coordinate set. The side chains of Glu 132, Glu 149, Lys 150, and Arg 499 were disordered and are not visible in the current map.

Chain Tracing and Folding. A ribbon representation of the pyruvate kinase subunit is displayed in Figure 3. As originally described in the structure of the enzyme from cat muscle (Stammers & Muirhead, 1975), the subunit of rabbit muscle pyruvate kinase can be divided into four distinct structural domains. Those amino acid residues participating in the formation of secondary structural elements are listed in Table 2. The N domain, defined by Ile 12–Arg 42, consists of a short helix–turn–helix motif. Domain A, composed of residues Asn 43–Gly 115 and Ala 219–Ala 387, follows the N-terminal domain. Domain A folds into a parallel $(\beta/\alpha)_8$-barrel motif. There are two additional α-helices in this domain. Domain B, bounded by Pro 116 and Pro 218, lies between the third β-strand and the third α-helix of domain A. This region of the polypeptide chain is characterized by nine β-strands that wrap around to form a β-barrel. Domain C, delineated by Met 388–Pro 530, consists of five α-helices and five strands of mixed β-sheet. Strands 1–4 run parallel to one another, while the fifth strand lies antiparallel in the sheet.

There are three regions where differences between the models of the rabbit and cat muscle pyruvate kinases are appreciable. First, the N-terminal α-helix in the model of rabbit muscle pyruvate kinase appears as an extended region of polypeptide chain in the model of the cat protein. Second, the overall topology of domain B differs in the models of the two proteins. A superposition of the α-carbon traces of the

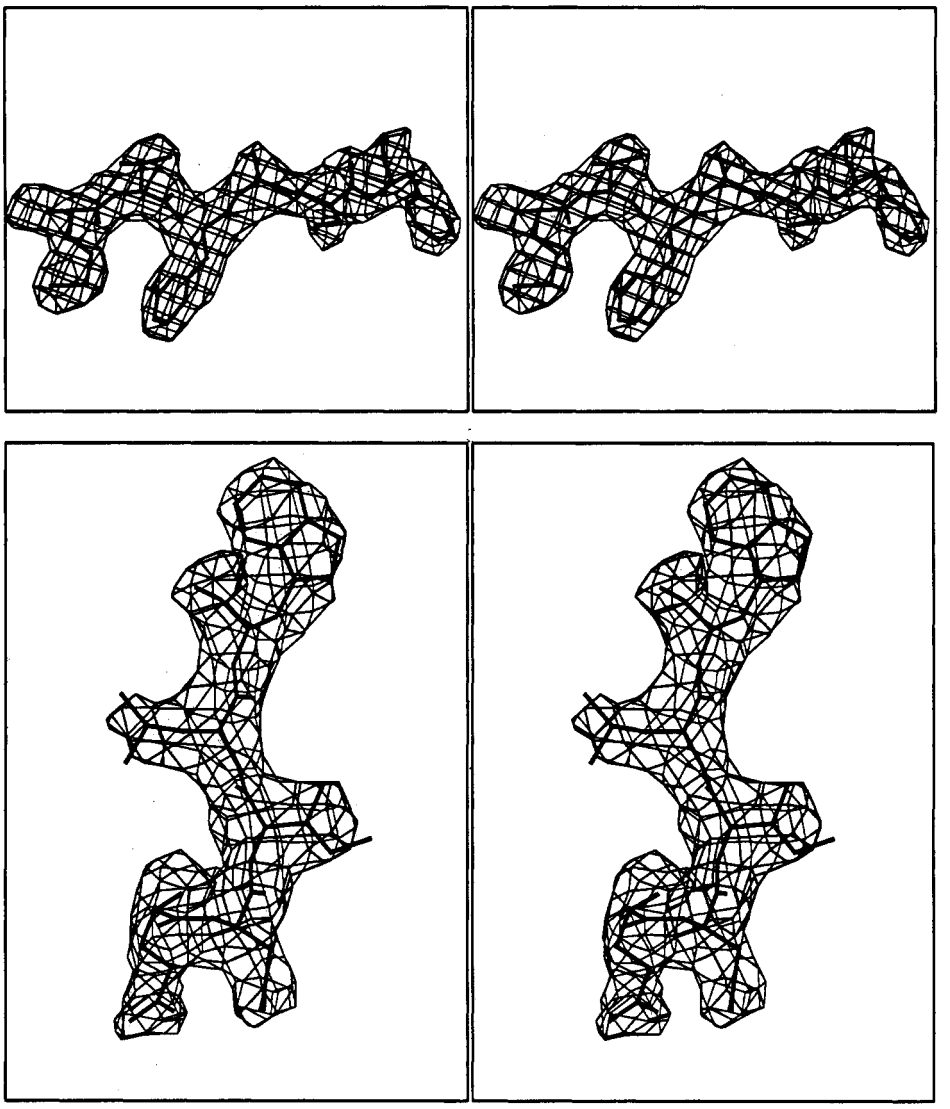

FIGURE 2: Representative portions of the electron density map. The averaged electron density maps shown here were contoured at 1σ. (a, top) Electron density for Met 238, Val 239, Phe 240, Ala 241, Ser 242, and Phe 243 in the A domain. (b, bottom) Electron density for Glu 153, Asn 154, Ile 155, Leu 156, and Trp 157 in the B domain.

rabbit and cat proteins in this region is shown in Figure 4. Finally, the course of the polypeptide chain between Lys 504 and the C-terminus differs such that the final two β-strands in the model from the cat protein run in the opposite direction of that observed in the rabbit enzyme structure, as can be seen in Figure 5. Due to this reversal, the C-termini of the two models do not superimpose.

Active Site. The active site is located in a cleft between domains A and B (Muirhead et al., 1986), and electron density associated with Mn^{2+} and pyruvate appears in this region of the map of the rabbit enzyme. The active site contains three positively charged side chains (Arg 72, Arg 119, and Lys 269) and four negatively charged residues (Asp 112, Glu 117, Glu 271, and Asp 295). As shown below, the carboxylates of Asp 112, Glu 271, and Asp 295 are ligands of the inorganic cofactors. Electron density corresponding to the Mn^{2+}–pyruvate complex is shown in Figure 6. A close-up view of the active site is shown in Figure 7.

The Divalent Cation Site. Mn^{2+} coordinates to the protein through the carboxylate side chains of Glu 271 and Asp 295. The presence of two protein ligands for the enzyme-bound Mn^{2+} is consistent with the coordination scheme for the enzyme–oxalate–Mn^{II}–ATP–Mg^{II} complex obtained from EPR spectroscopic data for the complex (Lodato & Reed, 1987). With the exception of Glu 271, this coordination scheme for the enzyme-bound divalent cation differs from the tentative scheme suggested for the cat enzyme (Muirhead et al., 1986). In the model of the cat enzyme, the side chain of Asp 295 was oriented away from the active site, and the main-chain carbonyls of Ala 292 and Arg 293 were suggested as probable ligands. The side chain of Arg 293 projects into the active site of the cat apoenzyme (Muirhead et al., 1986), whereas in the rabbit protein, this side chain projects away. Differences in the orientations of the side chains of Asp 295 and Arg 293 between the cat and rabbit structures may be a consequence of high concentrations of sulfate in the crystals of the cat protein.

Substrate Binding. Electron density corresponding to pyruvate is contiguous with that of Mn^{2+} (Figure 6). EPR spectroscopic data indicate that pyruvate chelates to Mn^{2+} through its carboxylate and carbonyl groups in complexes of enzyme–pyruvate–Mn^{II}–vanadate (Lodato, 1986) and in complexes of enzyme–pyruvate–Mn^{II}–ATP–Mg^{II} (Buchbinder, 1991). Pyruvate was therefore built into the density with this binding mode. The ϵ-NH_2 of Lys 269 and the OH of Thr 327 lie on opposite sides of the chelated pyruvate. As there are no other side chains in the vicinity that could function as general acid–base catalysts, pyruvate is tentatively oriented

FIGURE 3: Ribbon cartoon of the pyruvate kinase monomer. The subunit folds into four distinct structural domains: the N-terminal domain, which is located at the left side of the figure, the A domain, which lies in the middle of the figure, the B domain, which protrudes from the body of the molecule and is positioned at the top of the figure, and the C-terminal domain, which is situated at the bottom of the figure. Pyruvate, Mn^{2+}, and K^+ are depicted as space-filling models. This figure was prepared with the software package, MOLSCRIPT (Kraulis, 1991).

Table 2: Major Secondary Structural Elements

amino acid residue	type of structure
Leu 17–Met 21	α-helix
Phe 25–Cys 30	α-helix
Thr 44–Ile 50	β-sheet
Val 57–Ser 66	α-helix
Val 70–Asn 74	β-sheet
His 80–Thr 94	α-helix
Ala 108–Lys 114	β-sheet
Ile 118–Ile 123	β-sheet
Glu 132–Lys 135	β-sheet
Ala 137–Thr 142	β-sheet
Ile 155–Leu 158	β-sheet
Ser 171–Val 175	β-sheet
Ile 180–Gly 188	β-sheet
Phe 191–Val 196	β-sheet
Asn 198–Phe 201	β-sheet
Lys 206–Pro 211	β-sheet
Glu 222–Glu 234	α-helix
Met 238–Ser 242	β-sheet
Ala 248–Leu 257	α-helix
Lys 265–Ile 270	β-sheet
His 273–Arg 277	α-helix
Phe 279–Ala 285	α-helix
Gly 288–Ala 292	β-sheet
Arg 293–Glu 299	α-helix
Ala 302–Ala 319	α-helix
Lys 321–Ala 326	β-sheet
Glu 331–Ile 334	α-helical turn
Arg 341–Asp 353	α-helix
Cys 357–Leu 360	β-sheet
Pro 370–Ala 387	α-helix
His 390–Ser 400	α-helix
Leu 407–Lys 421	α-helix
Ala 426–Thr 431	β-sheet
Arg 435–Arg 442	α-helix
Ile 449–Thr 453	β-sheet
His 456–Leu 464	α-helix
Ile 468–Cys 473	β-sheet
Trp 481–Arg 499	α-helix
Val 507–Gly 513	β-sheet
Thr 523–Pro 528	β-sheet

with its methyl group between Thr 327 and Lys 269. In this orientation, the OH of Thr 327 would lie above the 2 *si* face of the double bond of the enolate, whereas the ϵ-NH_2 of Lys 269 would reside on the 2 *re* face of the double bond. Protonation of the enolate occurs stereospecifically from the 2 *si* face (Rose, 1970). Thus, O^{γ} of Thr 327 is positioned ~3 Å from the methyl carbon of pyruvate and on the 2 *si* face of the enolate.

Rose et al. (1991) have suggested that the proton donor in pyruvate kinase is a high-pK_a, monoprotic acid that rapidly exchanges protons with solvent in the unliganded enzyme. The OH of Thr 327 satisfies these requirements, as well as the stereochemistry. On the other hand, pH–rate profiles reveal an ionization with a pK_a of 8.3, and this ionization has been interpreted as the pK_a of the acid–base catalyst (Dougherty & Cleland, 1985). This pK_a is not inconsistent with that expected for the ϵ-NH_2 of Lys 269. It is known that the enolization of bound pyruvate requires a phosphate-like dianion as a cofactor (Rose, 1960), and it is possible that the relative positions of participants could change when a phosphate cofactor is bound. In the present structure, the OH of Thr 327 is not part of any visible network that might function as a proton relay (Rose et al., 1991), although ordered solvent cannot be excluded from such a function at the present resolution. The strict conservation of Thr 327 and Lys 269, as well as their critical positioning within the active site, implies that side chains associated with both residues participate in catalysis. In its present location, the protonated ϵ-amino group of Lys 269 could interact with the γ-phosphate of ATP. The γ-phosphate of ATP bridges the two divalent cations in the active site (Lodato & Reed, 1987). Recent stereochemical investigations suggest that the third peripheral oxygen of the γ-phosphate likely interacts with a positively charged group in the active site (Buchbinder et al., 1993). The side chain of Arg 72 is also a candidate for participation in binding of the phosphate moiety.

Oxalate, a potent inhibitor (Reed & Morgan, 1974) and pseudosubstrate (Kofron & Reed, 1990) of pyruvate kinase, is isostructural with the enolate of pyruvate. The carboxylate oxygen of oxalate, which would reside in a position analogous to that of the methyl group of pyruvate, could hydrogen bond to the OH of Thr 327 and to the ϵ-amino group of Lys 269. Such hydrogen-bonding interactions would contribute to the high binding affinity of oxalate for pyruvate kinase.

The Monovalent Cation Site. Stimulation of enzymatic activity by specific monovalent cations, initially discovered for pyruvate kinase (Boyer et al., 1942), has since been documented for several other enzymes (Suelter, 1970). Structural details of specific binding sites for alkali metal ions on proteins are of interest for this class of enzymes, as well as for the Na^+/K^+-ATPases (Robinson & Pratap, 1993). Toney et al. (1993) have recently described two distinct binding sites for alkali metal ions on the enzyme dialkylglycine decarboxylase. For pyruvate kinase, the ionic radius of the monovalent cation appears to be the important property in activation of the enzyme, and saturation of the binding site

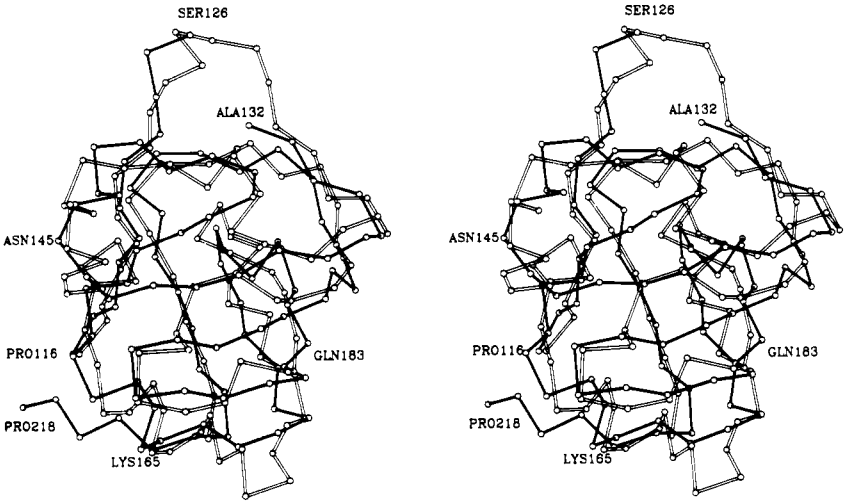

FIGURE 4: Superposition of the B domains from the rabbit and cat forms of pyruvate kinase. This figure was prepared with the software package, PLUTO, originally written by Dr. Sam Motherwell and modified for proteins by Drs. Eleanor Dodson and Phil Evans. These two domains were superimposed according to the algorithm of Rossmann and Argos (1975). The models of the rabbit and cat enzymes are displayed in solid and open bonds, respectively. Those amino acid residues that are labeled correspond to the protein from rabbit. In the rabbit pyruvate kinase model, there is a break in the electron density from Ser 126 to Glu 132.

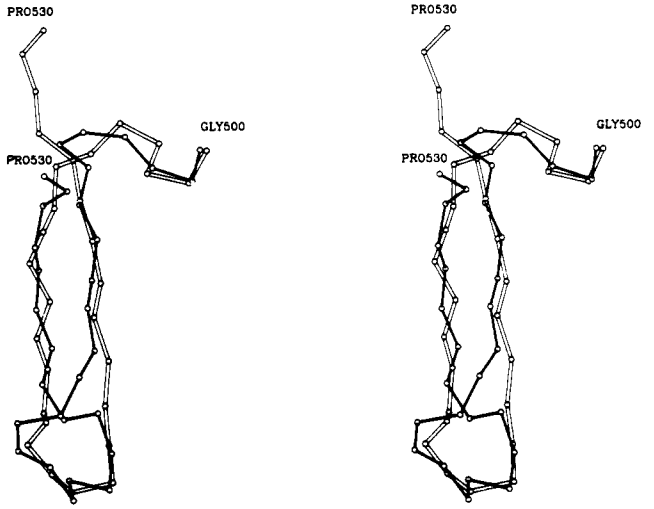

FIGURE 5: Superposition of the rabbit and cat pyruvate kinase models in the region defined by Gly 500–Pro 530. The topology of the β-strands in this region differs in the two proteins, such that the C-terminal amino acid residues do not superimpose. The rabbit and cat enzyme structures are depicted in solid and open bonds, respectively.

with a poorly activating cation (e.g., Na^+ or Li^+) fails to elicit full activation (Kayne, 1971).

In the map of rabbit pyruvate kinase, spherical electron density for K^+ appears in a well-defined site between the carbonyl oxygen of Thr 113, O^{γ} of Ser 76, $O^{\delta 1}$ of Asn 74, and $O^{\delta 2}$ of Asp 112, as shown in Figure 8. $O^{\delta 2}$ of Asp 112 may also hydrogen bond to the ϵ-amino group of Lys 269 and to $N^{\eta 2}$ of Arg 72. In addition, $O^{\delta 1}$ of Asp 112 is at H-bonding distance from N^{ϵ} of Arg 72. The separation between Mn^{2+} and K^+ is 5.7 Å. This intercation distance is slightly less than the NMR estimates for the Mn^{2+} to Tl^+ separation (6.8–8.2 Å) in the enzyme–Mn^{II}–Tl^I complex (Reuben & Kayne, 1971). Results from NMR relaxation measurements with Tl^+ (Reuben & Kayne, 1971) and other monovalent cations (Raushel & Villafranca, 1980) also indicated that the gap between Mn^{2+} and the monovalent cation closes to 4–5 Å in the complex with P-enolpyruvate.

As shown in Figure 7, K^+ does not interact directly with the bound pyruvate. The potential H-bonding interaction between the carboxylate of Asp 112 and the ϵ-amino of Lys 269 and the guanidinium of Arg 72 may provide an indirect linkage between K^+ and a catalytic group. Toney et al. (1993) have observed structural changes in the K^+ binding site in dialkylglycine decarboxylase when Na^+ is substituted for K^+. These changes are propagated to the vicinity of proposed catalytic groups and are likely responsible for the specificity of monovalent cation activation. In pyruvate kinase, the indirect linkage between K^+ and the ϵ-amino group of Lys 269 and the guanidinium of Arg 72 might be sufficient to account for the monovalent cation effects on the catalytic activity, although additional experiments are required to explore this conjecture.

Lord and Reed (1987) found that there are two sites for binding of Tl^+ in VO^{2+} complexes with pyruvate kinase. Binding of Tl^+ to the lower affinity site resulted in resolved superhyperfine splitting between the nuclear spin of $^{203,205}Tl^+$ and the unpaired electron of VO^{2+}, implying that the second site was very close to the vanadyl cation. It is not yet known whether the multiple sites for monovalent cations are unique to the VO^{2+}–Tl^+ complexes, but the existence of additional sites for K^+ cannot be ruled out.

Sequence Comparisons. There is a high degree of identity among the 20 known pyruvate kinase sequences in the region of the active site. Residues that are shown here to interact with the metal cofactors or that lie close to the bound pyruvate are part of strictly conserved motifs. For example, the two Mn^{2+} ligands, Glu 271 and Asp 295, are part of ^{268}SKIEN and ^{290}MVARGDLG motifs, respectively, that are strictly conserved. Lys 269 is part of the former sequence, and Thr 327 lies in a strictly conserved sequence, ^{326}ATQM. The four residues that contribute to the K^+ binding site, Asn 74, Ser 76, Asp 112, and Thr 113, lie in ^{74}NFSHG and ^{112}DTKGP motifs that are strictly conserved except for Thr 113 in one protein. Thr 113 is replaced by a Leu in the type II enzyme from *E. coli*. Because the main-chain carbonyl oxygen of Thr 113 is the ligand for K^+, this latter substitution might be conservative with respect to the K^+ binding site. The type II enzyme from *E. coli* is, however, not dependent on monovalent cations for activity (Waygood et al., 1975). The additional substitution of Lys for Glu 117 in the type II enzyme from *E. coli* is intriguing, given the strategic position of Glu 117 close to the K^+ site.

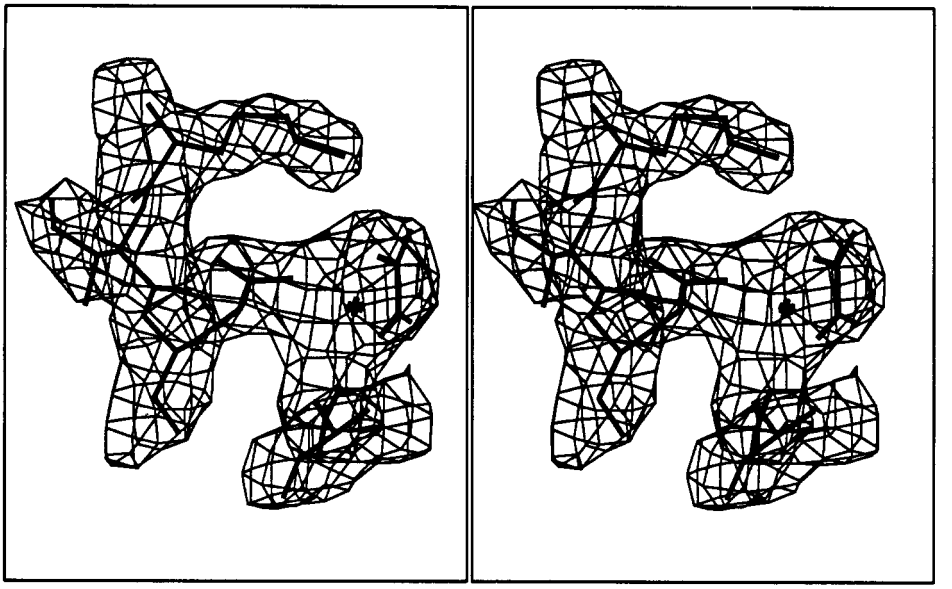

FIGURE 6: Electron density corresponding to the Mn^{2+}–pyruvate complex. The averaged electron density shown here was contoured at 1σ. The metal ion is coordinated by four oxygens: two donated by pyruvate and two provided by the carboxylates of Glu 271 and Asp 295. The other two ligands, which are not visible in the present map, are presumably water molecules. The maximum electron density at Mn^{2+} was 6σ compared to a maximum of 1.5σ for the surrounding protein.

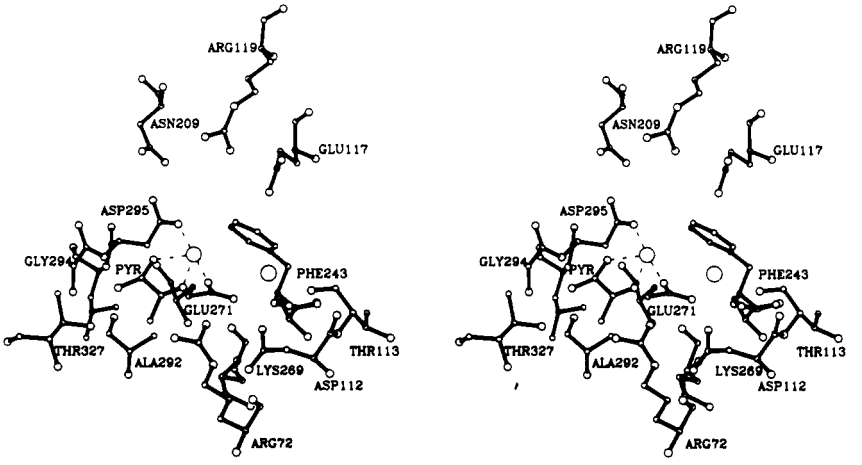

FIGURE 7: Stereoview of the active site of rabbit muscle pyruvate kinase. Amino acid residues Glu 117, Arg 119, and Asn 209 are located in the B domain; the other residues in the figure are from the A domain. The dashed lines indicate coordinate bonds between the oxygen ligands and Mn^{2+}. Both the Mn^{2+} and K^+ ions are depicted as open circles.

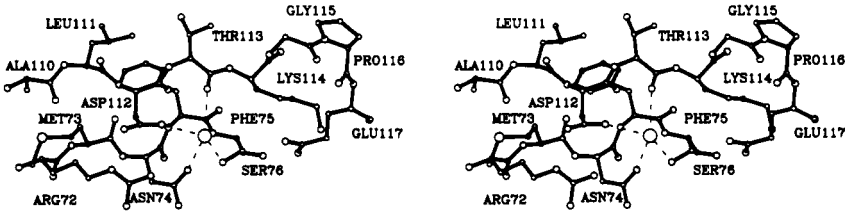

FIGURE 8: Close-up view of the K^+ binding site. Potential interactions between K^+ and the protein are indicated by the dashed lines. K^+ to oxygen distances are as follows: carbonyl O of Thr 113, 2.8 Å; O^{γ} of Ser 76, 2.9 Å; $O^{\delta 1}$ of Asn 74, 3.2 Å; and $O^{\delta 2}$ of Asp 112, 2.8 Å. The closest carboxylate oxygen from the side chain of Glu 117 is 4.7 Å from K^+. The maximum electron density at K^+ was 3σ, compared to a maximum of 1.5σ for the surrounding protein.

Perspective. The structural model obtained from crystals of this complexed form of rabbit muscle pyruvate kinase reveals the binding sites and ligands for the monovalent cation and one of the divalent cations in the active site. The model also focuses attention on the side chains of Thr 327, Lys 269, and Arg 72 as potential catalytic groups. The second divalent cation enters the active site with the nucleotide substrate (Gupta et al., 1976) and is, therefore, missing in the present structure. A structure for a complex containing all of the components or analogs thereof is obviously desirable to delineate further the positions of amino acid residues in the functional active site. The complex of enzyme, ATP, and oxalate (Lodato & Reed, 1987; Buchbinder & Reed, 1990; Buchbinder et al., 1993) is an attractive candidate for such structural investigations, and crystals of this complex are currently under investigation.

ACKNOWLEDGMENT

We thank Dr. C. Parkison for the clone of the rat muscle pyruvate kinase and Drs. Neil Madsen, W. Liu, and L.

deCastro for the rabbit muscle cDNA library. We also thank Michael Zuber and Dr. Bruce Jacobson for assistance and advice on cloning and Dr. Matthew Benning for assistance with computations. We are grateful to Dr. Hilary Muirhead for providing the coordinates of cat muscle pyruvate kinase.

REFERENCES

Ash, D. E., Goodhart, P. J., & Reed, G. H. (1984) *Arch. Biochem. Biophys. 228,* 31–40.
Baek, Y. H., & Nowak, T. (1982) *Arch. Biochem. Biophys. 217,* 491–497.
Bernstein, F. C., Koetzle, T. E., Williams, G. J. B., Meyer, E. F., Jr., Brice, M. D., Rogers, J. R., Kennard, O., Shimanouchi, T., & Tasumi, M. (1977) *J. Mol. Biol. 112,* 535–542.
Boyer, P. D. (1962) in *The Enzymes*, 2nd ed. (Boyer, P. D., Lardy, H., & Myrbäck, K., Eds.) Vol. 6, pp 95–113, Academic Press, New York.
Boyer, P. D., Lardy, H. A., & Phillips, P. H. (1942) *J. Biol. Chem. 146,* 673–682.
Bricogne, G. (1976) *Acta. Crystallogr. A, 32,* 832–847.
Buchbinder, J. L. (1991) Ph.D. Dissertation, University of Wisconsin—Madison, Madison, WI.
Buchbinder, J. L., & Reed, G. H. (1990) *Biochemistry 29,* 1799–1806.
Buchbinder, J. L., Baraniak, J., Frey, P. A., & Reed, G. H. (1993) *Biochemistry 32,* 14111–14116.
Carminatti, H., Jimenez de Asua, L., Leiderman, B., & Rozengurt, E. (1971) *J. Biol. Chem. 246,* 7284–7288.
Creighton, D. J., & Rose, I. A. (1976) *J. Biol. Chem. 251,* 61–68.
Devereux, J., Haeberli, P., & Smithies, O. (1984) *Nucleic Acids Res. 12,* 387–395.
Dougherty, T. M., & Cleland, W. W. (1985) *Biochemistry 24,* 5875–5880.
Fitzgerald, P. M. (1988) *J. Appl. Crystallogr. 21,* 273–278.
Fox, G. C., & Holmes, K. C. (1966) *Acta Crystallogr. 20,* 886–891.
Gupta, R. K., & Mildvan, A. S. (1977) *J. Biol. Chem. 252,* 5967–5976.
Gupta, R. K., Oesterling, R. M., & Mildvan, A. S. (1976) *Biochemistry 15,* 2881–2887.
Hall, E. R., & Cottam, G. L. (1978) *Int. J. Biochem. 9,* 785–793.
Jones, T. A. (1985) *Methods Enzymol. 115,* 157–171.
Kabsch, W. (1988a) *J. Appl. Crystallogr. 21,* 67–71.
Kabsch, W. (1988b) *J. Appl. Crystallogr. 21,* 916–924.
Kayne, F. J. (1971) *Arch. Biochem. Biophys. 143,* 232–239.
Kayne, F. J. (1973) in *The Enzymes*, 3rd ed. (Boyer, P. D., Ed.) Vol. 8, pp 353–382, Academic Press, New York.
Kayne, F. J. (1974) *Biochem. Biophys. Res. Commun. 59,* 8–13.
Kofron, J. L., & Reed, G. H. (1990) *Arch. Biochem. Biophys. 280,* 40–44.
Kraulis, P. J. (1991) *J. Appl. Crystallogr. 24,* 946–950.
Kuo, D. J., & Rose, I. A. (1978) *J. Am. Chem. Soc. 100,* 6288–6289.
Kuo, D. J., O'Connell, E. L., & Rose, I. A. (1979) *J. Am. Chem. Soc. 101,* 5025–5030.
Kupiecki, F. P., & Coon, M. J. (1960) *J. Biol. Chem. 235,* 1944–1947.
Ljungstrom, O., Hjelmquist, G., & Engstrom, L., (1976) *FEBS Lett. 56,* 288–292.
Lodato, D. T. (1986) Ph.D. Dissertation, University of Pennsylvania, Philadelphia, PA.
Lodato, D. T., & Reed, G. H. (1987) *Biochemistry 26,* 2243–2250.
Lord, K. A., & Reed, G. H. (1987) *Inorg. Chem. 26,* 1464–1466.
Muirhead, H., Claydon, D. A., Barford, D., Lorimer, C. G., Fothergill-Gilmore, L. A., Schiltz, E., & Schmitt, W. (1986) *EMBO J. 5,* 475–481.
Muirhead, H., Clayden, D. A., Cuffe, S. P., & Davies, C., (1987) *Biochem. Soc. Trans. 15,* 996–999.
Nowak, T., & Suelter, C. H. (1981) *Mol. Cell. Biochem. 35,* 65–75.
Parkison, C., Ashizawa, K., McPhie, P., Lin, K.-H., & Cheng, S.-Y. (1991) *Biochem. Biophys. Res. Commun. 179,* 668–674.
Raushel, F. M., & Villafranca, J. J. (1980) *Biochemistry 19,* 5481–5485.
Read, R. J. (1986) *Acta Crystallogr. A 42,* 140–149.
Reed, G. H., & Morgan, S. D. (1974) *Biochemistry 13,* 3537–3541.
Reuben, J., & Kayne, F. J. (1971) *J. Biol. Chem. 246,* 6227–6234.
Robinson, J. D., & Pratap, P. R. (1993) *Biochim. Biophys. Acta 1154,* 83–104.
Rose, I. A. (1960) *J. Biol. Chem. 235,* 1170–1177.
Rose, I. A. (1970) *J. Biol. Chem. 245,* 6052–6056.
Rose, I. A., & Kuo, D. J. (1989) *Biochemistry 28,* 9579–9585.
Rose, I. A., Kuo, D. J., & Warms, J. V. B. (1991) *Biochemistry 30,* 722–726.
Rossmann, M. G., & Argos, P. (1975) *J. Biol. Chem. 250,* 7525–7532.
Sambrook, J., Fritsch, E. F., & Maniatis, T. (1989) *Molecular Cloning: A Laboratory Manual,* 2nd ed., Cold Spring Harbor Laboratory Press, Cold Spring Harbor, NY.
Schmidt-Bäse, K., Buchbinder, J. L., Reed, G. H., & Rayment, I. (1991) *Proteins: Struct., Funct., Genet. 11,* 153–157.
Seeholzer, S. H., Jaworowski, A., & Rose, I. A. (1991) *Biochemistry 30,* 727–732.
Short, J. M., Fernandez, J. M., Sorge, J. A., & Huse, W. D. (1988) *Nucleic Acids Res. 16,* 7583–7600.
Stammers, D. K., & Muirhead, H. (1975) *J. Mol. Biol. 95,* 213–225.
Stuart, D. I., Levine, M., Muirhead, H., & Stammers, D. K. (1979) *J. Mol. Biol. 134,* 109–142.
Suelter, C. H. (1970) *Science 168,* 789–795.
Tietz, A., & Ochoa, S. (1958) *Arch. Biochem. Biophys. 78,* 477–493.
Toney, M. D., Hohenester, E., Cowan, S. W., & Jansonius, J. N. (1993) *Science 261,* 756–759.
Tronrud, D. E., Ten Eyck, L. F., & Mattews, B. W. (1987) *Acta Crystallogr. A 43,* 489–501.
Waygood, E. B, Rayman, M. K., & Sanwal, B. D. (1975) *Can. J. Biochem. 53,* 444–454.
Weiss, P. M., Hermes, J. D., Dougherty, T. M., & Cle'and, W. W. (1984) *Biochemistry 23,* 4346–4350.